IMPACT DAMAGE TO 3D WOVEN CFRP COMPOSITE PLATES

G. Zumpano[1,3], MPF Sutcliffe[1], C Monroy Aceves[1], WJ Stronge[1], M. Fox[2]
[1]Cambridge University Engineering Department
Trumpington Street, Cambridge, CB2 1PZ, U.K.
[2] School of Materials, Manchester University,
Paper Science Building, Sackville Street, Manchester, M60 1QD, U.K
[3] Currently at Rolls-Royce plc, PO Box 31, Derby, DE24 8BJ, England
mpfs@eng.cam.ac.uk (MPF Sutcliffe)

SUMMARY

A glass-carbon hybrid braided composite and two CFRP 3D woven composites with orthogonal weave and a layer-to-layer weave are impacted with hemispherically-tipped impactors, using a gas gun at energies up to 60 J. The damage area, as measured by ultrasonic C-scanning, increases roughly linearly with impact energy, while the peak contact force increases roughly as the square root of the impact energy. Sectioning is used to examine damage details. Although some large delaminations are observed, there are significant areas free of larger cracks, which nevertheless show damage under C-scanning, presumably due to microcracking.

Keywords: Woven, 3D, braided, impact, C-scan, sectioning

INTRODUCTION

Composite materials are widely used in high value applications requiring good specific stiffness and strength. However, there is a tendency for these materials to suffer more damage as a result of impact than equivalent metallic materials. This damage is either in the form of fracture of the relatively brittle fibres or due to cracking in the matrix [1]. Woven materials have traditionally been used in impact-critical applications due to their superior ability, relative to unidirectional composites, to maintain structural integrity under significant impact energies. 3D woven materials combine the attractive properties of traditional woven materials, but in addition contain tows through the thickness, which can play a role in containing any delamination between the layers.

In general there are at least two phases of impact damage in composites: (1) dynamic compaction of the composite plate as it is compressed at the impaction site; and (2) delamination of plies in the neighbourhood of the impact site [2]. The exact nature of damage will depend on the details of the weave architecture, resin and fibre properties and the geometry and energy of the colliding impactor [1, 3]. However, at low energies impact damage tends to be in the form of bending damage on the distal surface and an approximately circular internal delamination. At high incident energies fibre splitting, perforation or shear failure occurs [4]. Damage tends to initiate on the distal surface if the ratio of plate thickness to projectile nose radius is less than one and on the impact surface if the plate thickness is greater than the projectile radius [3, 5].

Three approaches can be used to increase the impact resistance of composites. Use of improved weave architecture, specifically 3D woven material, can be used to introduce through-thickness tows, which tend to hold the material together at the impact site and so reduce delamination damage. Through thickness tows in three-dimensional weaves can act as crack stoppers by altering the fracture paths from intra-tow mode to inter-ply mode; this approximately doubles the fracture toughness [6]. Alternatively, tougher resins can be used to increase the delamination toughness and so improve the composite impact resistance [7]. Finally use of ductile glass fibres in place of some of the relatively brittle carbon fibres can be used to increase the strain to failure of the material and hence potentially increase the impact resistance, at the expense of increased weight and reduced stiffness. These mixtures are called hybrid composites.

Previous work by the authors [8] has examined low and high speed impacts of braided hybrid material, exploring the effects of impact energy on surface damage and C-scanned damage area. In this paper we further explore the mechanisms causing failure in these hybrid samples, and compare the results with impact tests on two 3D woven materials.

METHODOLOGY

Materials

Two 3D woven CFRP composites, an orthogonal weave and a layer-to-layer weave, were supplied for testing. In addition these materials were compared with a braided hybrid textile with an overall fibre volume fraction of 51%, of which 75% was high strength carbon fibres and the remaining 25% glass fibres. The carbon and glass fibres were braided in a 2×2 twill weave; four layers were used to make the composite. Dry preforms of all materials were resin transfer moulded with epoxy resin to form flat plates of a nominal thickness of 4.5 mm. These were C-scanned to identify any poor quality regions, which were not used.

Testing procedure

Square plates with side length either 130 mm or 200 mm were cut out for impact testing and mounted in a rigid support frame. Steel hemispherical-ended impactors of tip radius 6.25 mm and masses either 12.5 or 21.4 grammes were projected normally at the plates using a gas gun at impact speeds between 35 and 70 m/s. In fact, results presented below showed no significant effect of plate size, with the majority of results presented being for the smaller plate size. Moreover, by plotting results as a function of impact energy, no significant differences are observed between the two impactor masses. Hence no differentiation is made in the presentation between these different experimental conditions.

High speed photography was used to measure the impact and rebound speeds, and the contact force, as described in the next section. Further details of the methodology are given in [8].

Image analysis

High speed photography was used to capture the impact event. The location of the impactor, as a function of time, was identified from the images using a purpose-written Matlab code. The blunt trailing edge of the impactor was used as a reference edge to track the position of the impactor. This edge was detected by locating the maximum intensity gradient in the image. The position of this edge was then differentiated twice numerically with respect to time to find the velocity and acceleration (taking deceleration as positive). The force was inferred by multiplying the acceleration by the impactor mass. A quadratic fit to the acceleration near the peak was used to improve the accuracy of the inferred peak force. Fig. 1 shows the results of the procedure, illustrating the reasonable accuracy of the acceleration estimate (as evidenced by the small scatter in the acceleration before impact and the smooth form of the curves, at least until the contact is lost).

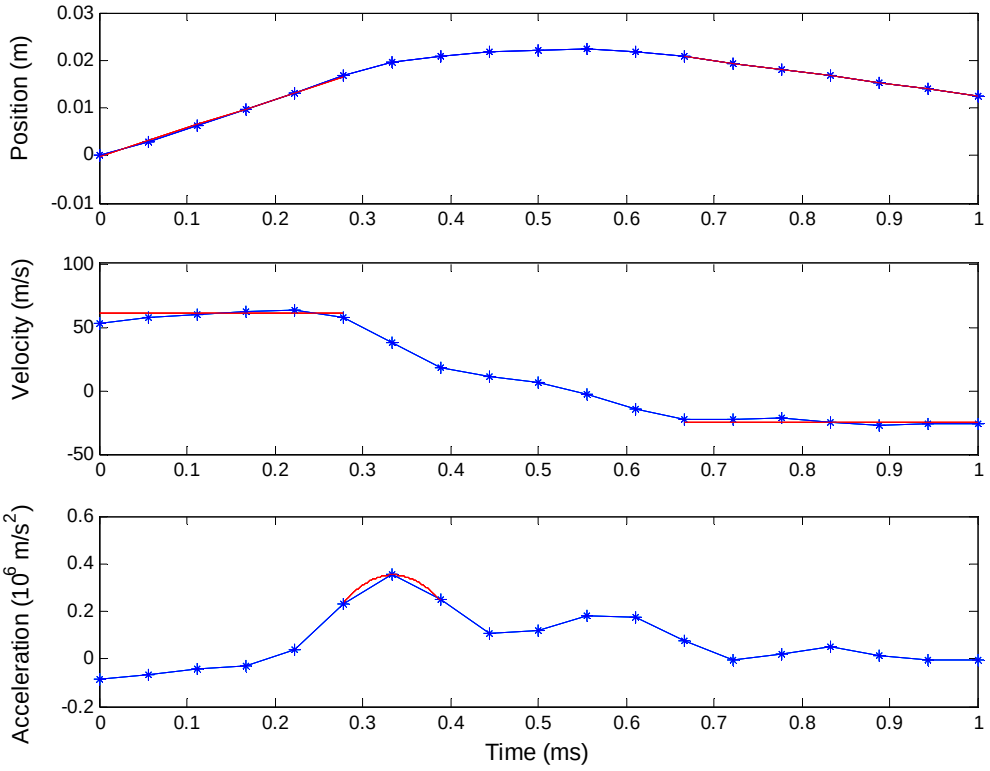

Figure 1. High speed photography analysis of position, velocity and acceleration of impactor for braided specimen, m = 21.4g, impact energy = 39 J. Red lines show corresponding curve fits.

Damage Detection

Damage to the plates was assessed by C-scan and by sectioning. Ultrasonic C-scanning was undertaken using a MIDAS NDT water-jet inspection system, using an unfocussed 5 MHz probe in transmission mode and a 50 mm/s scan rate. There was a clear division in the C-scan intensity between the undamaged regions of the plate and a roughly circular region around the impact site. The damage area was found from the area above a suitable intensity threshold. Figure 2 illustrates the impact site and corresponding C-scan image of a braided sample. Red and yellow rectangles superimposed on the photograph identify the footprint of carbon and glass tows, respectively. Surface damage is observed on the photograph, while a roughly circular patch of damage is revealed by C-scanning.

Sections of the braided material were used to identify the extent and type of damage. Figure 3 shows schematically how the specimen was sliced using a Struers Accutom-50 to make a series of sections through the damage area. The samples were polished and imaged using a BX51 Olympus microscope with an automatic stage. A section was also gold coated and viewed in a scanning electron microscope (SEM).

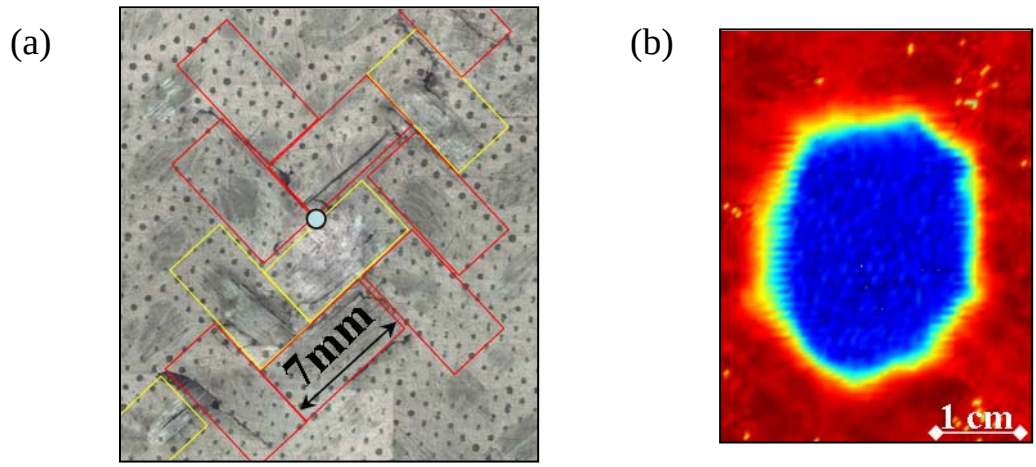

Figure 2. Damage in a braided sample impacted by a 21.5 g projectile with an impact energy of 33 J; (a) micrograph of impact surface. Yellow and red rectangles identify glass and carbon tows, respectively. The blue circle shows the impact site, (b) C-scan.

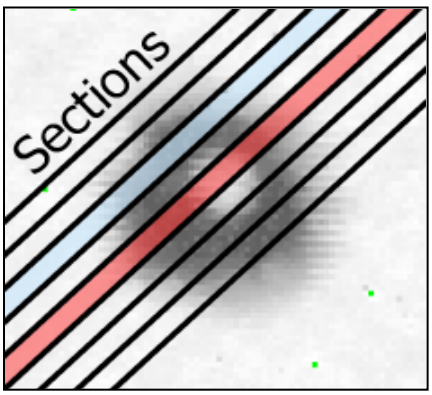

Figure 3. Schematic of the sections cut from the impacted area of a braided sample (impact energy 12 J), overlaid on the C-scan image. Blue section – no clearly visible damage. Red section – clearly visible damage.

RESULTS

Absorbed energy

Figure 4 shows the variation of absorbed energy with impact energy for the three materials tested. The diagonal black line is where the absorbed energy equals the impact energy. The closeness of all the data to this line shows that there was rather a small amount of energy in the rebounding impactor (in none of the tests did the impactor penetrate the plate). Some of the absorbed energy is dissipated in the form of inelastic damage, but some is also dissipated during the subsequent oscillatory motion of the plate, after the impactor has lost contact with the plate. The hybrid braided material absorbs slightly less energy than the CFRP 3D woven composites.

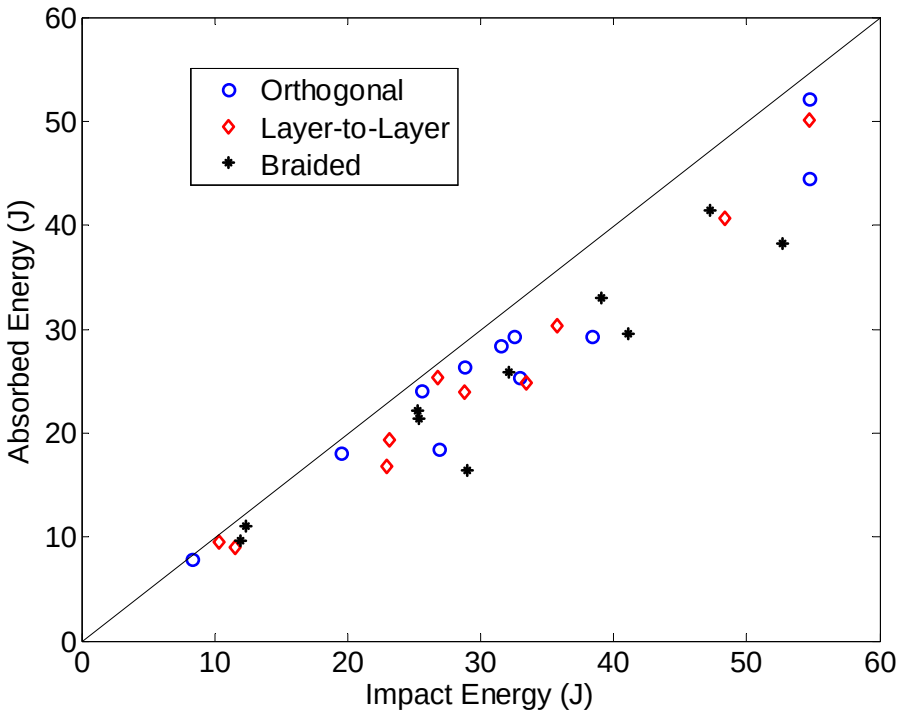

Figure 4. Variation of absorbed energy with impact energy.

Contact force

Figure 5 shows the variation of maximum contact force with impact energy. Contact force could only be inferred for the larger masses, because the smaller impactors were obscured at the point of impact by the plate support structure. Results for the three different materials are roughly similar, though there is more scatter in the hybrid material than in the two CFRP woven materials. It has been suggested [8] that this variability is due to differences when either glass or carbon tows are struck by the tip of the impactor.

Assuming that the plate behaves in a linear elastic manner, with a stiffness k relating the contact force F and the central plate deflection δ, equating the impact kinetic energy E_I with the stored elastic energy in the plate at maximum deflection gives a relationship for the maximum contact F_m as

$$F_m = \sqrt{2k\,E_I} \tag{1}$$

Now the stiffness of a centrally loaded fully clamped square plate of side length L and thickness t, made of isotropic material with an elastic modulus E and Poisson's ratio 0.3, is given by [9] as

$$k = \frac{Et^3}{0.0611L^2} \tag{2}$$

Figure 5 shows that a square root relation between impact energy and contact force, of the form given in (1), gives a good fit to the data. However the corresponding modulus E for this curve fit is 6 GPa, well below a typical elastic modulus for such materials [10]. Since inertial effects would increase the effective stiffness of the plate, this finding suggests that, at least for the impact conditions considered, local strains transverse to the loading direction (e.g. associated with damage at the impact site) are significantly reducing the contact force. This is consistent with the observation of dimples left in the plate at the impact site.

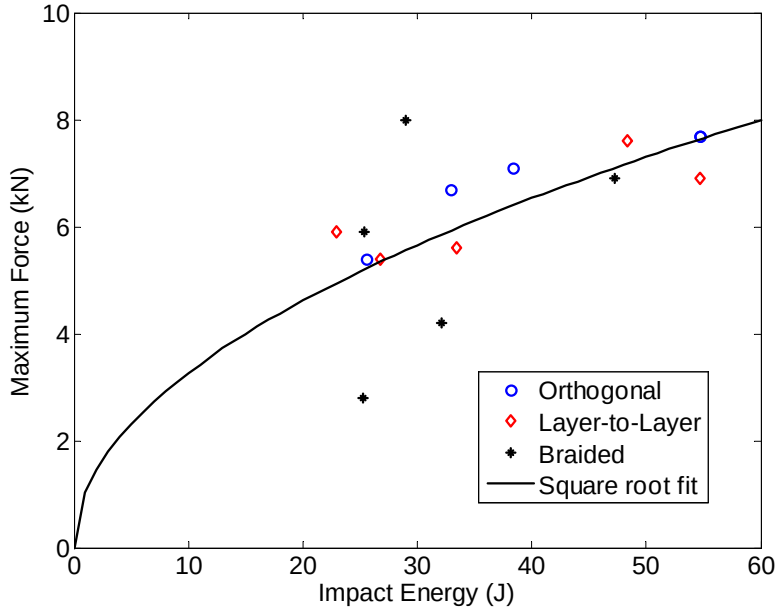

Figure 5. Variation of maximum contact force with impact energy.

Damage area

Figure 6 shows the variation with impact energy of the damage area detected by C-scanning. The contact area increases roughly linearly with the impact energy, for a given material. The damage areas for the two 3D woven materials are comparable, but significantly larger than that seen in the braided material at corresponding energies. This is despite the contact forces being similar for the three materials.

As noted earlier, no significant differences were observed between the smaller and larger plates, and between the two impactor masses; hence these different cases have not been differentiated in Fig. 6. Evidently, for these impact conditions, the impact energy is an appropriate way to characterise the impact conditions, while effects of clamping conditions are not significant.

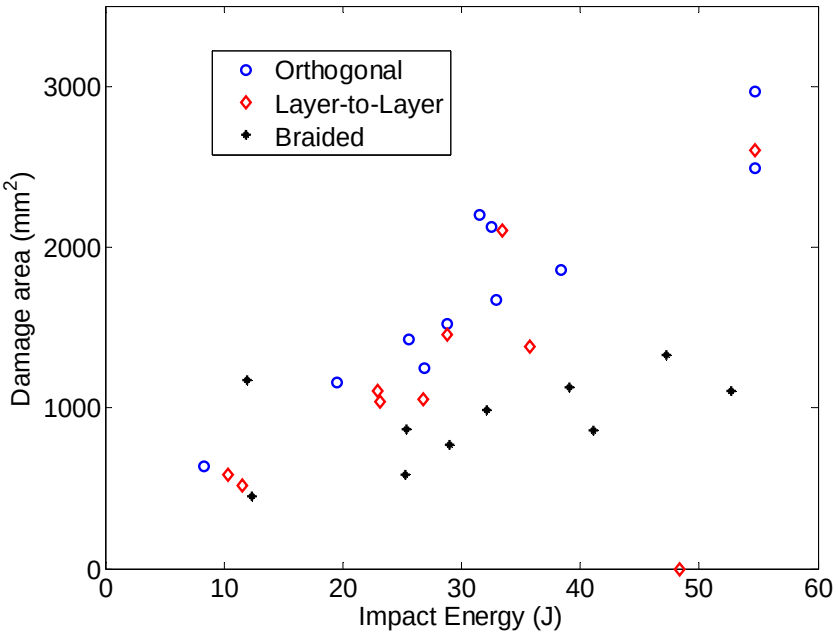

Figure 6. Variation with impact energy of damage area, as assessed by C-scanning.

Microscopy

Sections were taken from the braided samples to identify the modes of failure in the impact region. It was expected that large delaminations would be seen, corresponding to the damage area identified in the C-scanning (see for example Fig 2). In fact this was not the case. While in a few sections there were large delaminations spanning the length of the damage area seen in the C-scans, there were also extensive regions where rather little damage was observed on the sections using optical imaging. For example, considering the series of sections shown in Fig 3. for a braided sample, only the red section directly under the impactor had such large delaminations while the section identified in blue in Fig. 3 had no such delaminations, despite being well within the

damage area identified by C-scanning. Smaller damage on a tow scale was observed in other areas, see for example the smaller tow-splitting cracks seen in Fig. 7. However there were other areas where even such cracks were not present. Observation of such a section using a SEM did not reveal extensive cracking. In the absence of larger scale cracks being observed, it is supposed that the C-scan damage detected is associated with microcracks, perhaps at a fibre scale. It is possible that such microcracks might be seen in higher magnification imaging in the SEM, but careful surface preparation would be needed to avoid obscuring such features.

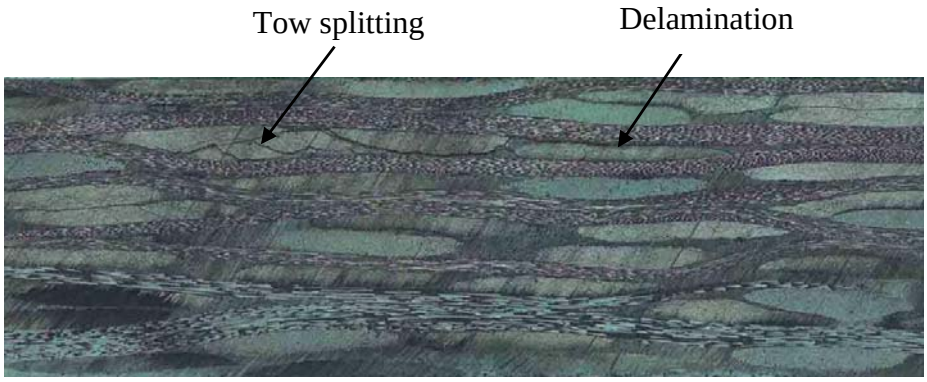

Figure 7. Optical micrograph of the cross-section of a braided sample within the damage area. Results are for the same sample illustrated in Fig. 3 with an impact energy of 12 J.

Conclusions

A glass-carbon hybrid braided composite and two CFRP 3D woven composites with orthogonal weave and a layer-to-layer weave were impacted with hemispherically-tipped impactors, using a gas gun at energies up to 60 J. By characterising the impact event by the impact energy, results were insensitive to the plate size or the impactor mass, within the range studied. Almost all the impact energy was absorbed by the plate, either in the form of inelastic damage or transferred as elastic energy and kinetic energy into the plate, being dissipated during subsequent motion of the plate. The peak contact force was estimated from the deceleration of the impactor, measured by high speed photography. The peak force increased roughly as the square root of the impact energy. A simple statics model of the impact event shows such a square root behaviour, but the corresponding effective plate bending stiffness was much lower than values expected for such materials. It was suggested that the reduced stiffness is due to transverse straining and local damage. The damage area, as measured by ultrasonic C-scanning, increased roughly linearly with impact energy. The two woven materials had similar areas of damage, but both had significantly more damage at corresponding impact energies than the braided material. Sectioning was used to examine damage details. Although some large delaminations were observed, there were significant areas free of larger cracks, which nevertheless showed damage under C-scanning. It is presumed that in this case C-scanning was detecting damage due to microcracking.

Acknowledgements
Contributions are gratefully acknowledged from the Engineering and Physical Sciences Research Council (grant EP/C538145/1), University of Nottingham, Cranfield University, Rolls-Royce Group plc., Dowty Propellers (Part of GE's Aviation Business), Carr Reinforcements Ltd., Laser Optical Engineering Ltd. and JR Technology Ltd.

References

1. N Tarim, F Findik, H Uzun. Ballistic impact performance of composite structures, *Composite Structures*, **56**, 13–20 (2002)

2. AP Mouritz. Ballistic impact and explosive blast resistance of stitched composites, *Composite: Part B*, **32**, 431-439 (2001)

3. SA Matemilola, WJ Stronge. Impact induced dynamic deformation and stresses in CFRP composite laminates. *Composites Engineering*, **5**, 211-222 (1995)

4. LS Sutherland, C Guedes Soares, Effects of laminate thickness and reinforcement type on the impact behaviour of E-glass/polyester laminates, Composites Science and Technology, **59**, 2243-2260 (1999)

5 WJ Cantwell, J Morton. Impact perforation of carbon fiber reinforced plastic. *Composites Science and Technology*, **38**, 119–41 (1990)

6. YA Bahei-El-Din, MA Zikry. Impact-induced deformation fields in 2D and 3D woven composites. *Composites Science Technology*, **63**(7), 923–42 (2003)

7. T Ebeling, A Hiltner, E Baer, IM Fraser, ML Orton. Delamination failure of a woven glass fiber composite, *Journal Composite Materials*, **31**, 1318–33 (1997)

8 C Thanomsilp, PJ Hogg. Penetration impact resistance of hybrid composites based on commingled yarn fabrics, *Composites Science and Technology*, **63**, 467–482 (2003)

9. G Zumpano, M Fox, WJ Stronge, MPF Sutcliffe. Impact damage in hybrid braided twill composites. *J Materials Science*, **43**(20) 6668-6675 (2008)

10. WR Young. *Roarks' formulas for stress and strain, 6th Edition. McGraw-Hill* page 464 (1989)

11. P Tan, L Tong, GP Stevens, T Ishikawa. Behavior of 3D orthogonal woven CFRP composites. Part I. Experimental investigation. *Composites Part A,* **31** 259-271 (2000)